Electronic Supplementary Information (ESI)

[24]Crown-8-modified carbon nanotubes for templating metal deposition and active materials for pseudocapacitors

Ruitao Zhou,[1†] Fung Kit Tang,[1†] Raymond Wai-Yin Sun,[2] Man Kin Tse,[2] Yujie Chen,[2] Albert Sun-Chi Chan,[2] Shengzhou Chen,[3] Xunjin Zhu,[1*] Ken Cham-Fai Leung[1*]

[1]Department of Chemistry, The Hong Kong Baptist University, Kowloon Tong, Kowloon, Hong Kong SAR, P. R. China

[2]Guangzhou Lee & Man Technology Company Limited, 8 Huanshi Avenue, Nansha, Guangzhou, P. R. China

[3]School of Chemistry and Chemical Engineering, Guangzhou University, Guangzhou, P. R. China

E-mail: cfleung@hkbu.edu.hk; xjzhu@hkbu.edu.hk

Section1: Experimental

Preparation and modification of oxidized MWCNT

0.5 g multi-walled CNT (30~50 nm in diameter, 10~30 μm in length) was immersed in 40 ml mixture of concentrated sulphuric acid and nitric acid (H_2SO_4: HNO_3 = 3:1 (v/v)) for 4 h in a sonication bath. The oxidized CNT was collected by filtration, washed with water and then EtOH. The oxidized CNT was further dried in vacuum overnight at room temperature. Oxidized CNT was further modified by dibenzo[24]crown-8-CH_2NH_2 (**DB24C8-CH_2NH_2**). The synthesis of **DB24C8-CH_2NH_2** was described in details in the supporting information. Briefly, 102 mg oxidized CNT was suspended in a 20 mL CH_2Cl_2 solution containing 1 mL $SOCl_2$. The mixture was stirred at room temperature for 2 h. Then 42.5 mg DB24C8-CH_2NH_2 in 5 mL CH_2Cl_2 was added. The resulting mixture was further stirred overnight at room temperature. Solvent was removed and the residue solid was washed with MeCN (20 mL x3), water (20 mL x5) and EtOH (20 mL x5). The solid was dried in vacuum, and 84.1 mg black powder was obtained. The crown ether-modified CNT was abbreviated as c-CNT in the following text.

Deposition of Nickel film on oxidized CNT and c-CNT

50 mg oxidized CNT (c-CNT) was immersed in 50 ml 1 % (w/w) silver nitrate solution for 15 min in an ultrasonication bath operating at 45 kHz with mechanical stirring. Then the CNT (c-CNT) was collected by vacuum assisted filtration and rinsed with de-ionized water twice. The resulting CNT (c-CNT) was transferred into 500 ml aqueous solution containing 4 g nickel sulphate, 2 g sodium citrate, 1 g lactic acid. The solution was mixed by mechanical

stirring for 15 min in an ultrasonication bath, and the pH of the solution was adjusted in the range of 7~9 by ammonia solution. Ultrasound was used to improve the dispersion of nanotubes in the ELD process for increasing deposition weight. Then a certain amount of 10 % (w/w) dimethylamine borane solution (1~10 mL) was added into the reaction solution according to the desired structure of the final nickel coated CNT. After 2 h, the resulting CNT@Ni (c-CNT@Ni) was collected by vacuum filtration and dried in vacuum at room temperature.

Synthesis of CNT@Ni-Fe@Fe_2O_3

CNT@Ni-Fe was synthesized by sequential deposition of Ni and Fe layer on CNT, and CNT@Ni-Fe@Fe_2O_3 was synthesized by surface oxidation of CNT@Ni-Fe in H_2O_2. The freshly synthesized CNT@Ni can directly catalyse the autocatalytic deposition of Fe. Briefly, 0.4 g CNT@Ni power was dispersed in 500 ml aqueous solution containing 1.15 g $FeSO_4 \cdot 7H_2O$，0.88 g sodium citrate and 0.5 g lactic acid. 25 ml 10 % (w/w) dimethylamine borane solution and 0.5 mL ammonia was gradually added into the above solution. The ELD deposition was carried out at 40 ˚C in an ultrasonication bath under sweep mode for 2 h. Ultrasound was used to remove the bubbles generated on the nanotubes. The resulting CNT@Ni-Fe was collected by filtration and dried in vacuum overnight. Oxidation of CNT@Ni-Fe was carried out by immersing the sample in 5 % (w/w) H_2O_2 solution for 4 h. Finally, CNT@Ni-Fe@Fe_2O_3 was synthesized.

Structural characterization

The process of synthesizing nickel layer on CNT was characterized by X-ray photoelectron spectroscopy (XPS, SKL-12) and energy dispersive spectroscopy (EDX). The structure of CNT@Ni was characterized by field emission scanning microscopy (FESEM, LEO 1530) and transmission electron microscopy (TEM, Tecnai G2 20 S-TWIN). The specific surface areas of CNT and CNT@Ni were characterized by Brunauer–Emmett–Teller (BET, ASAP2020) test. The structural and weight change of CNT@Ni during the electrochemical oxidation process was characterized by X-ray diffraction (XRD, Bruker AXS D8) and vibrating-sample magnetometer (VSM) tests, respectively.

The amount of oxidized Ni during the charge-discharge process was calculated through vibrating-sample magnetometer (VSM) curves by the following equations:

$$R_N = R_{N0}\frac{M}{M_0} \quad (1)$$

$$R_{Nh} = 0.9385\left(1 - \frac{M}{M_0}\right) \quad (2)$$

$$P = \frac{0.5942\left(1-\frac{M}{M_0}\right)}{R_{N0}\frac{M}{M_0}+0.5942\left(1-\frac{M}{M_0}\right)} \quad (3)$$

Where R_{N0} is the quantity of Ni(0) in 1 g raw sample, R_N is the quantity of Ni(0) in 1 g partly oxidized sample, M_0 is the saturation moment for 1 g raw sample by VSM test, M is the saturation moment for 1 g oxidized sample by VSM test, R_{Nh} is the quantity of nickel hydroxide in 1 g oxidized sample, P is the ratio of nickel that was oxidized. The nickel loading for the CNT@Ni sample is 90.6%.

Electrochemical characterization

The electrochemical performance of CNT@Ni was characterized in a three-electrode cell

with 1.5 M NaOH as the electrolyte by an electrochemical station (CHI660E), and Ag/AgCl and a platinum wire were used as the reference electrode and counter electrode, respectively. The working electrode was fabricated by pasting CNT@Ni slurry on a piece of nickel coated cloth with an area of 1 cm^2. Freestanding CNT@Ni plates were formed by hydrolytic force, and were also tested as working electrodes. To characterize the electrochemical performance of CNT@Ni electrodes, cyclic voltammetry (CV), galvanostatic charge-discharge (GCD) and electro impedance spectroscopy (EIS) tests were carried out.

The electrochemical performance of CNT@Ni@Fe@Fe_2O_3 was characterized in a three electrode cell with the procedure similar to that of CNT@Ni. An asymmetric supercapacitor was assembled by using CNT@Ni plate as the positive electrode and CNT@Ni-Fe@Fe_2O_3 plate as the negative electrode, and 1.5 M NaOH was used as the electrolyte. The electrochemical performance of the supercapacitor was tested under two-electrode mode. Flexible solid supercapacitors were also fabricated by compressing active materials on nickel cloth, and NaOH/polyethylene glycol hydrogel was used as the electrolyte.

The capacitance of electrodes and asymmetric supercapacitors was calculated through galvanostatic charge-discharge (GCD) curves by the following equations:

$$C_{vp} = It/v\Delta V \quad (4)$$

$$C_{sp} = It/s\Delta V \quad (5)$$

where C_{vp} is the volumetric capacitance, C_{sp} is the areal capacitance, I is the discharging current, t is the discharge time, v is the volume of the electrode, s is the area of the electrode,

and ΔV is the max discharging potential after the IR drop.

The energy density of the asymmetric supercapacitors by GCD curves is calculated by the equation:

$$E = I \int_0^t U_{(t)} dt \qquad (6)$$

where E is the energy density, t is the discharge time and $U_{(t)}$ is the discharge potential.

Section 2: Synthesis of crown ether moiety

*Synthesis of **2***

Both compounds **1** and **2** were synthesized according to the literature with modified procedures.[1] Compound **1 (**15.74 g, 42 mmol) was dissolved in 272 mL CH_2Cl_2 containing 22 mL triethylamine and 0.5 g catalytic amount of 4-dimethylaminopyridine. The solution was cooled in ice bath, and then *p*-toluenesulfonyl chloride (16.8 g, 88 mmol) in 100 mL CH_2Cl_2 was added dropwisely. The resulting mixture was stirred at room temperature for 24 h. The organic layer was washed with 1 M HCl solution (150 mL x2) and water (200 mL x3). The organic layer was collected and dried with anhydrous $MgSO_4$. The organic layer was concentrated and the product was purified by a silica gel column using EtOAc/*n*-hexane = 1:1 *v/v* → pure EtOAc as eluent. The product was obtained as a pale yellow liquid. Yield: 19.2 g, 67 %.^{1}H NMR (400 MHz, $CDCl_3$, 298 K) δ 7.78 (d, *J* = 8.3 Hz, 4H), 7.32 (d, *J* = 8.0 Hz, 4H), 6.90 (s, 4H), 4.18 – 4.10 (m, 8H), 3.86 – 3.77 (m, 4H), 3.72 – 3.64 (m, 8H), 3.62 – 3.56 (m, 4H), 2.42 (s, 6H). ^{13}C NMR (101 MHz, $CDCl_3$, 298K) δ 149.04 , 144.92 , 133.06 , 129.95 , 128.08 , 121.77 , 114.95 , 70.92 , 70.87 , 69.94 , 69.40 , 68.92 , 68.82 , 21.76 .

*Synthesis of **3***

Compound **3** has been reported in the literature.[2] Compound **2** (8.6 g, 12.5 mmol), Cs_2CO_3 (4.1 g, 12.7 mmol) and K_2CO_3 (7.1 g, 51 mmol) was added in 250 mL MeCN. Upon refluxing with stirring, 3,4-dihydroxybenzonitrile (1.7 g, 12.6 mmol) in 250 mL was added dropwisely from an additional funnel. The mixture was refluxed for 24 h. Insoluble materials was filtered and the filtrate was collected, the filtrate was collected and concentrated. The product was purified by silica gel column using pure EtOAc as eluent to yield a white solid.

Yield: 4.0 g, 67.5%. ^{1}H NMR (400 MHz, $CDCl_3$, 298K) δ 7.23 (dd, *J* = 8.3, 1.9 Hz, 1H), 7.06 (d, *J* = 1.9 Hz, 1H), 6.93 – 6.82 (m, 5H), 4.19 – 4.11 (m, 8H), 3.96 – 3.89 (m, 8H), 3.85 – 3.79 (m, 8H). ^{13}C NMR (101 MHz, $CDCl_3$, 298 K) δ 152.91, 148.96, 148.93, 126.83, 121.56, 121.51, 119.34, 116.29, 114.00, 113.98, 112.93, 104.11, 71.67, 71.59, 71.45, 70.08, 69.80, 69.74, 69.61, 69.52, 69.50, 69.43.

Synthesis of ***DB24C8-CH$_2$NH$_2$***

DB24C8-CH$_2$NH$_2$ has been reported in the literature.[3] Compound **3** (4 g, 8.4 mmol) was dissolved in 150 mL THF and the solution was cooled in an ice bath. Then $LiAlH_4$ (0.7 g, 18.4 mmol) was added to the solution. The mixture was slowly warmed to room temperature with stirring for 1 h. The mixture was refluxed for overnight. The mixture was cooled in ice bath, water was added dropwise until no bubbles was given out. The mixture was filtered through a sintered glass funnel and filtrate was collected. The filtrate was concentrated, the residue was diluted with water and extracted with EtOAc (100 mL x5). The organic layer was dried with anhydrous Na_2SO_4, the product was then purified by silica gel column using CH_2Cl_2/MeOH = 10:1 *v/v* as eluent to give a pale yellow solid. Yield: 1.66 g, 41.1%. ^{1}H NMR (400 MHz, $CDCl_3$, 298K) δ 6.87 – 6.79 (m, 5H), 6.77 (s, 2H), 4.18 – 4.06 (m, 8H), 3.90 – 3.84 (m, 8H), 3.79 (d, *J* = 1.2 Hz, 8H), 3.73 (s, 2H). ^{13}C NMR (101 MHz, $CDCl_3$, 298 K) δ 148.90, 148.84, 147.62, 136.60, 121.31, 119.56, 114.06, 114.00, 113.00, 71.17, 71.14, 69.84, 69.82, 69.51, 69.32, 69.30, 46.06.

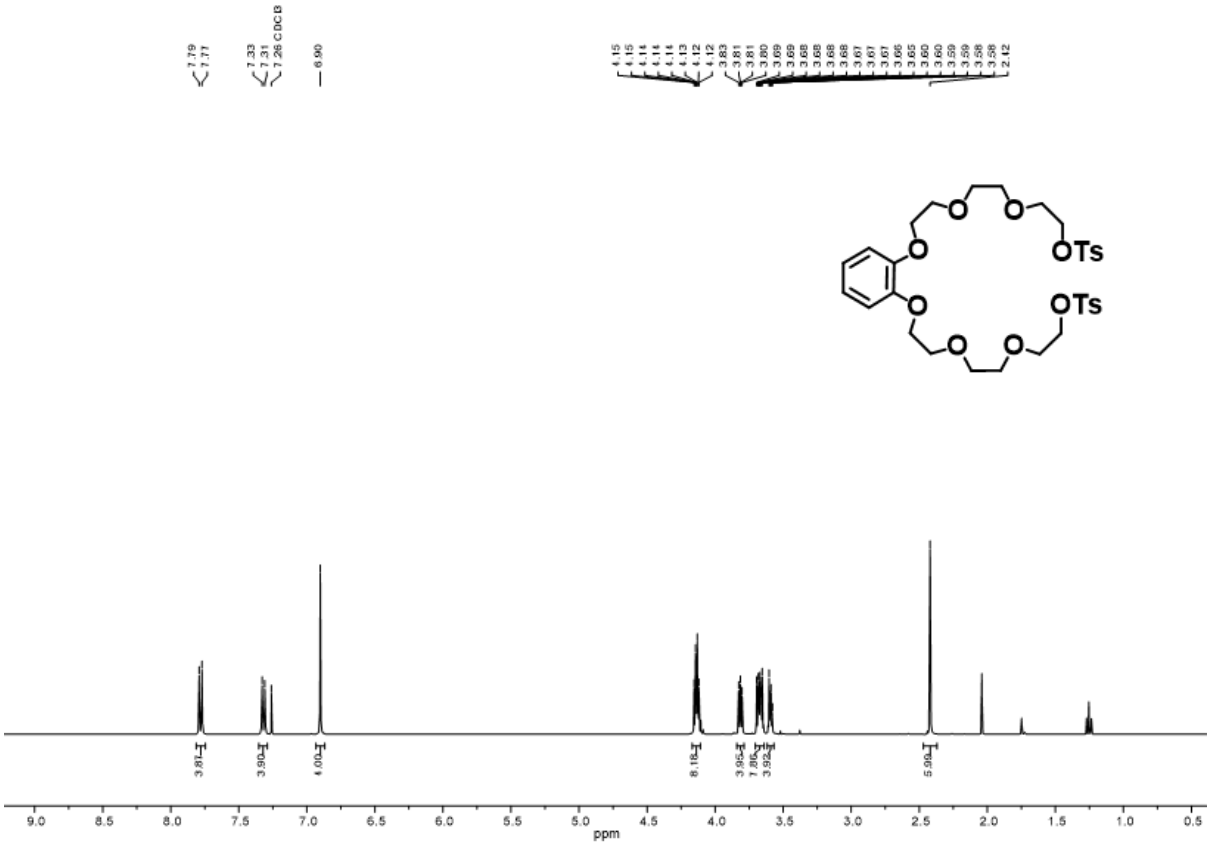

Fig. S1. ^{1}H NMR spectrum (400 MHz, $CDCl_3$, 298 K) of compound **2**.

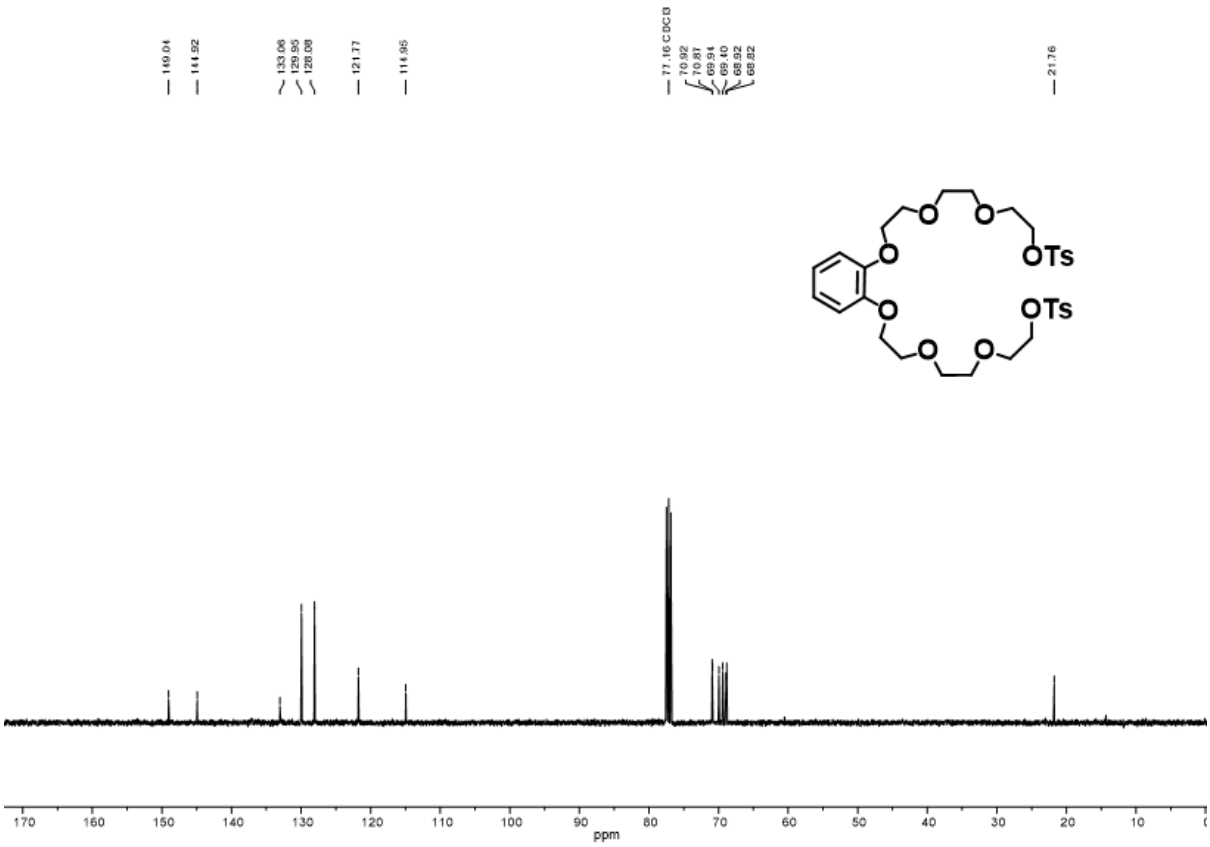

Fig. S2. $^{13}C\{^{1}H\}$ NMR spectrum (101 MHz, $CDCl_3$, 298 K) of compound **2**.

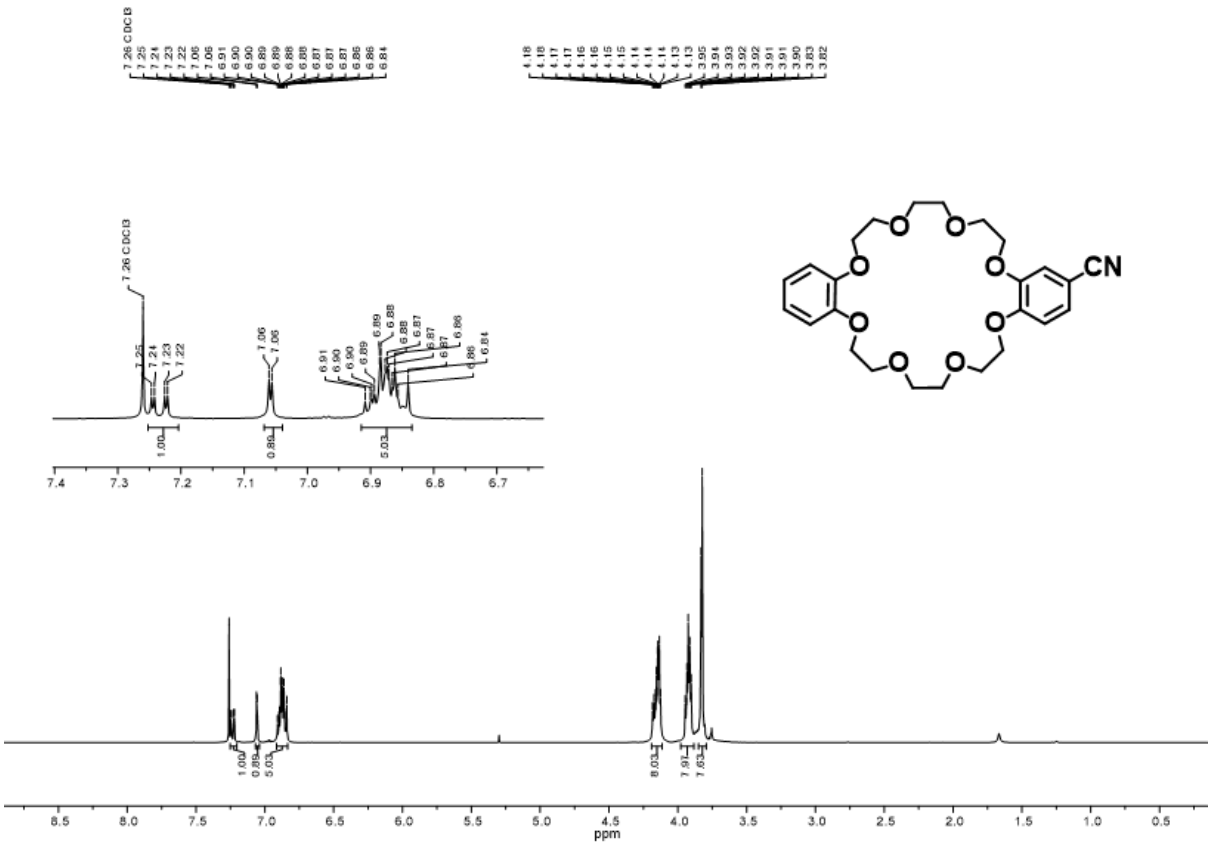

Fig. S3. ^{1}H NMR spectrum (400 MHz, $CDCl_3$, 298 K) of compound **3**.

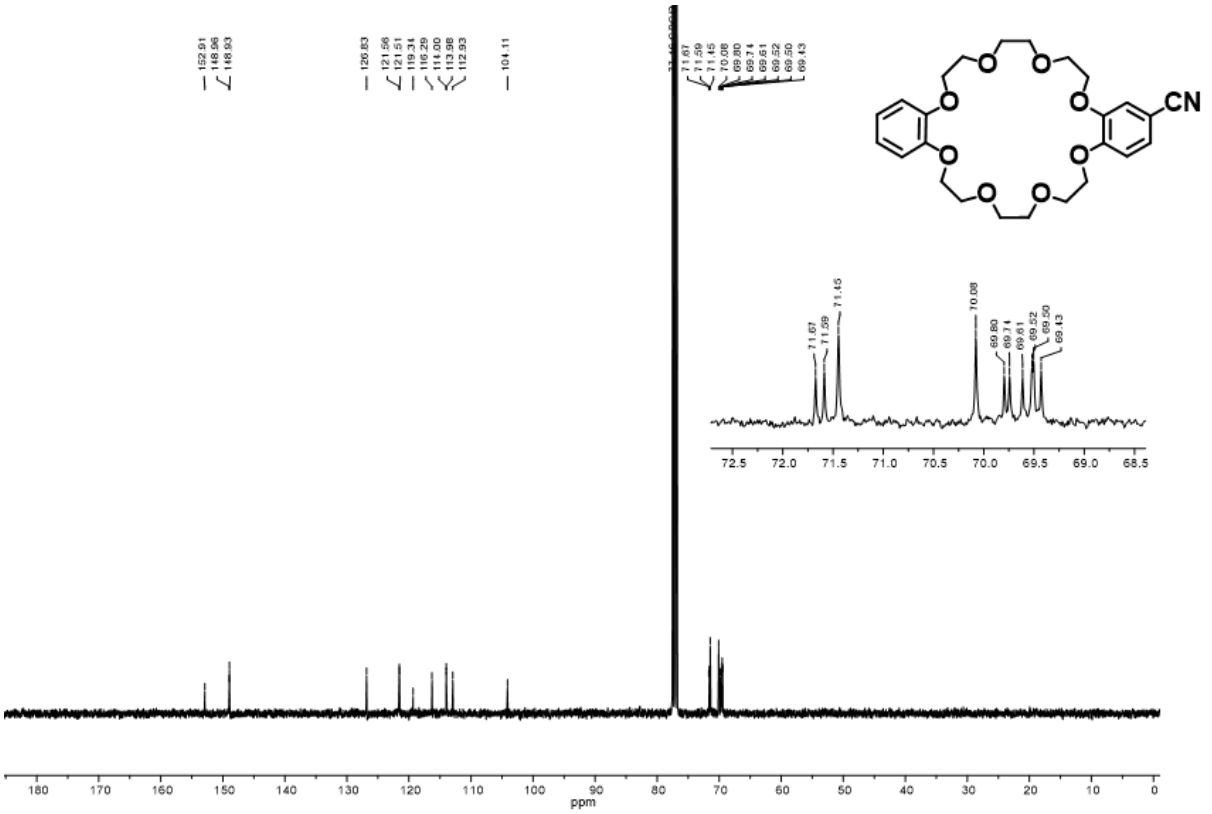

Fig. S4. $^{13}C\{^{1}H\}$ NMR spectrum (101 MHz, $CDCl_3$, 298 K) of compound **3**.

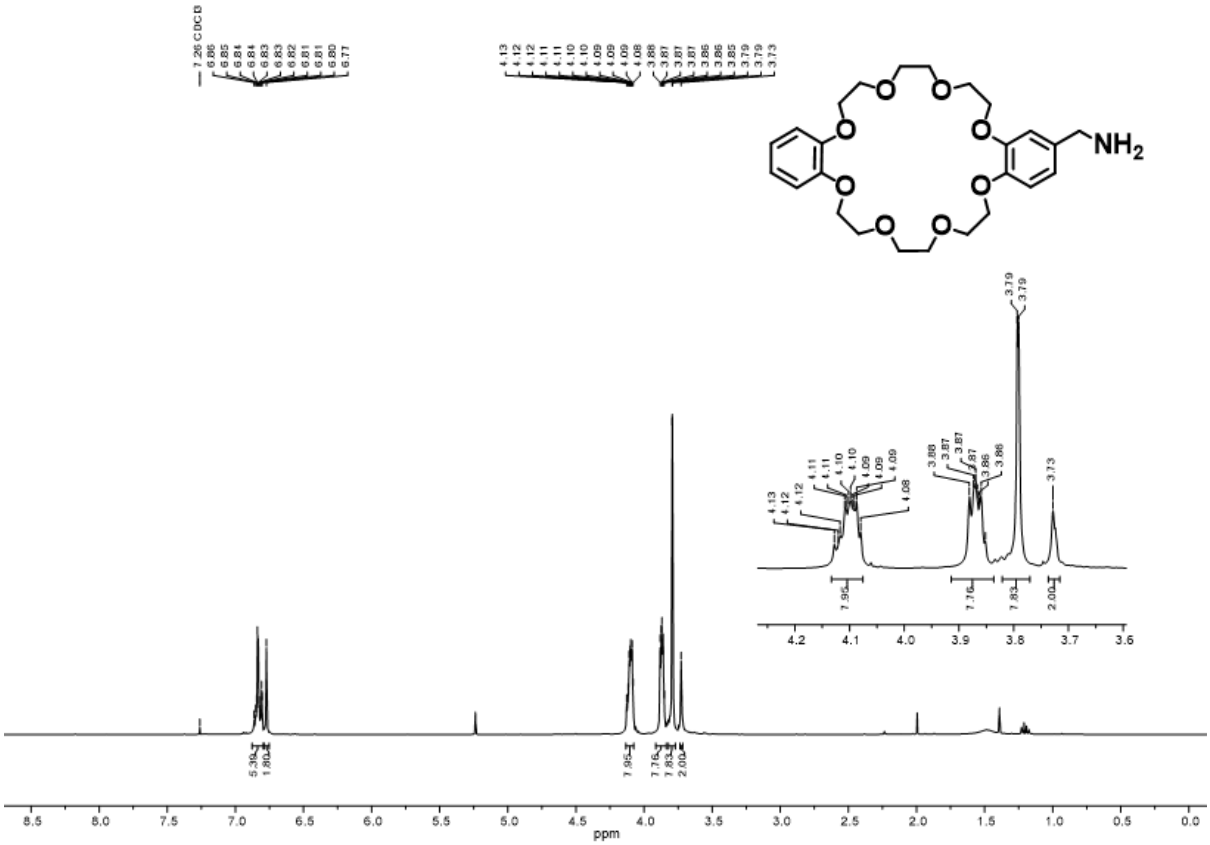

Fig. S5. ^{1}H NMR spectrum (400 MHz, $CDCl_3$, 298 K) of ***DB24C8-CH$_2$NH$_2$***.

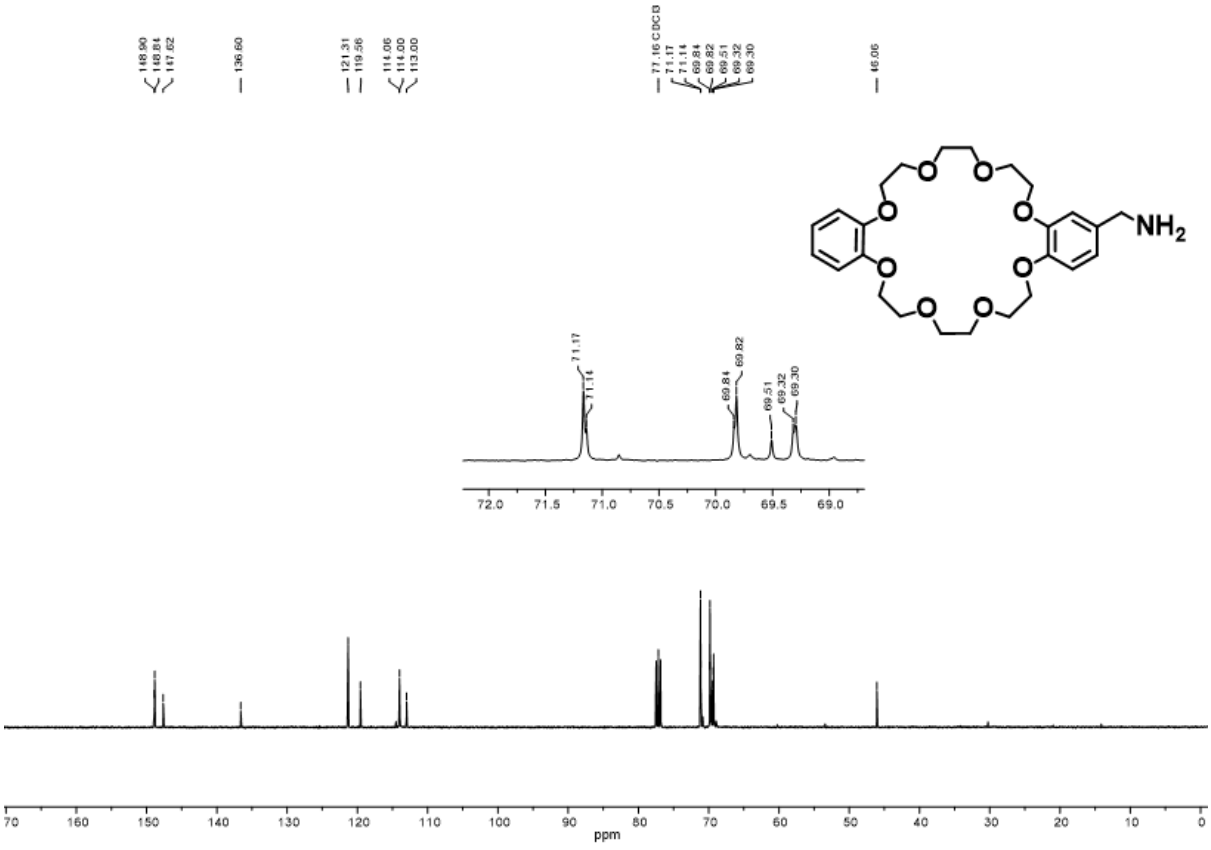

Fig. S6. $^{13}C\{^{1}H\}$ NMR spectrum (101 MHz, $CDCl_3$, 298 K) of ***DB24C8-CH$_2$NH$_2$***.

Section 3: Additional graphs, microscopic images and spectra

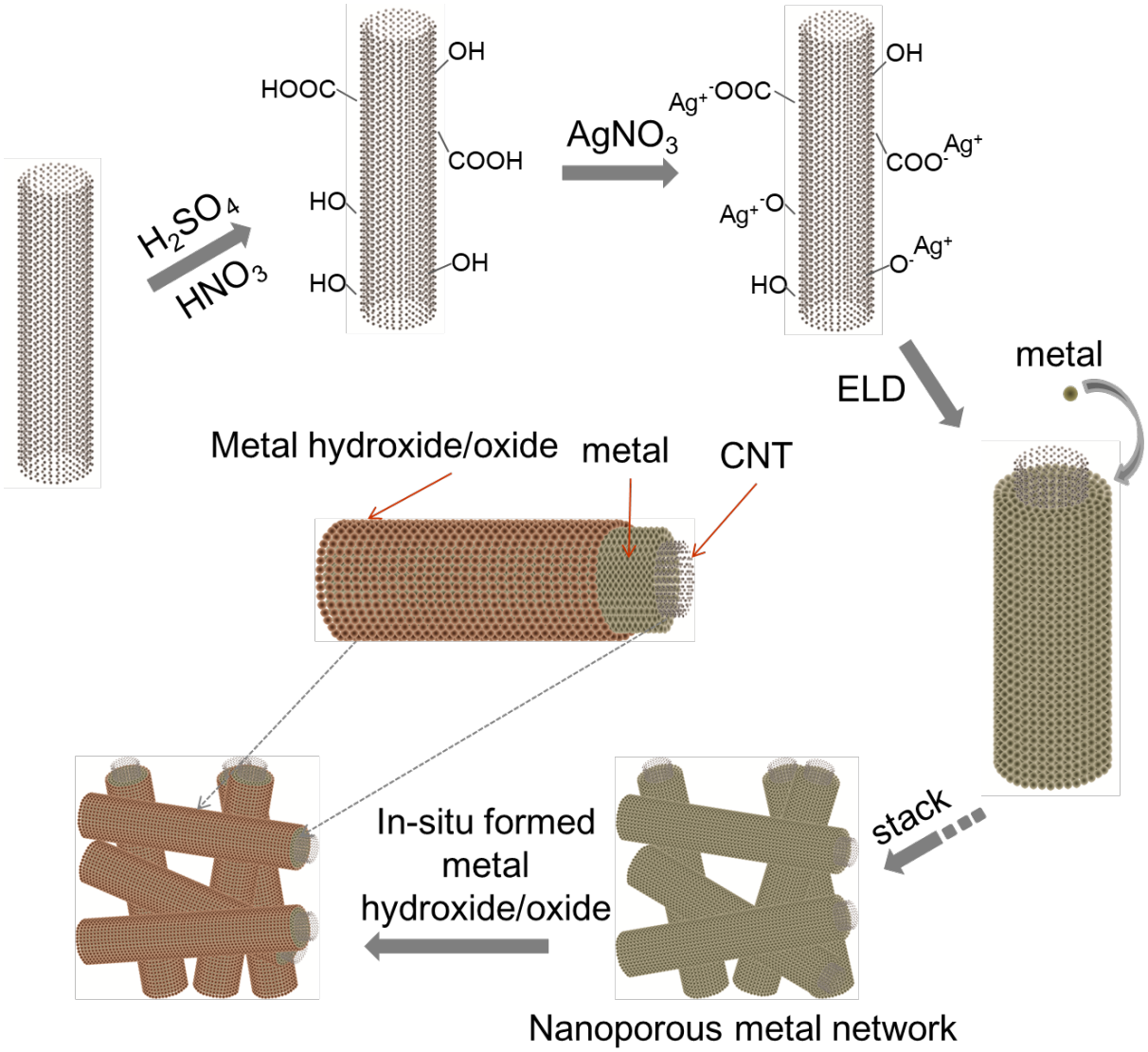

Fig. S7 Scheme of the synthetic process of freestanding CNT@Ni@$Ni(OH)_2$ electrodes.

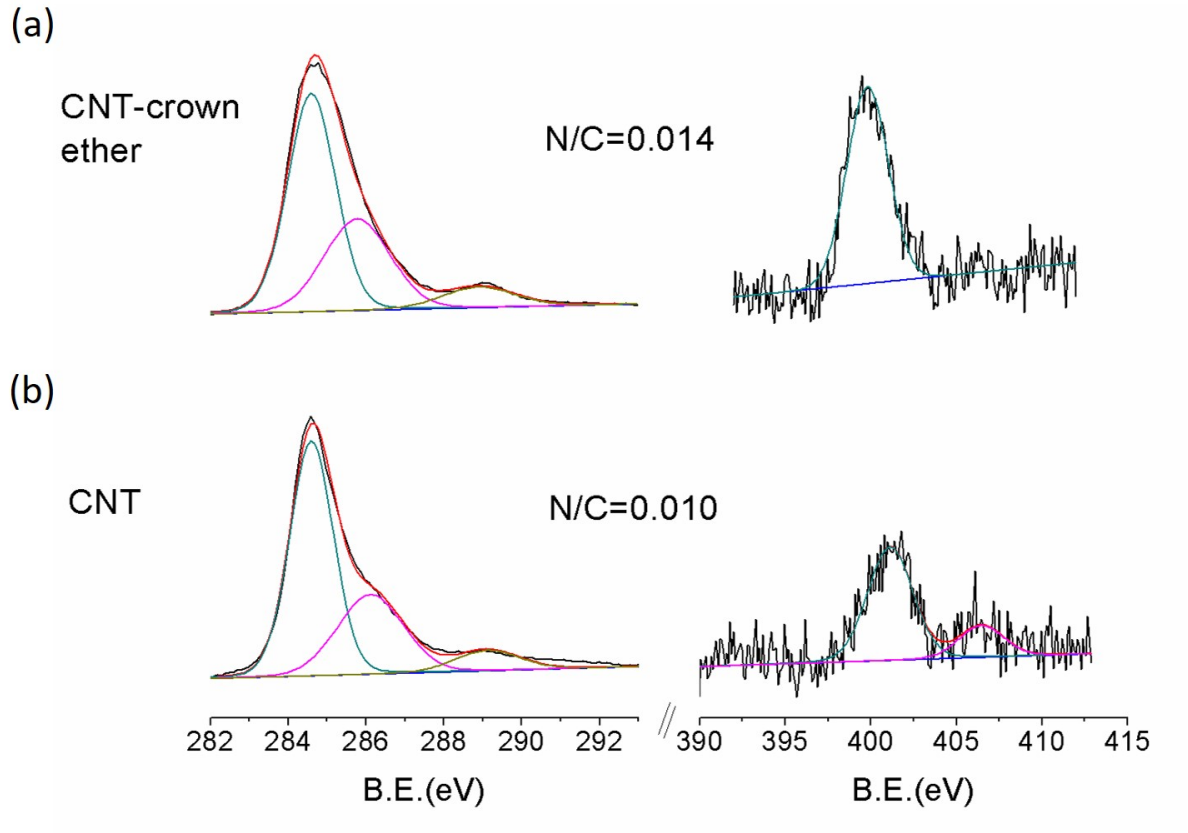

Fig. S8 XPS analyses of (a) c-CNT and (b) CNT.

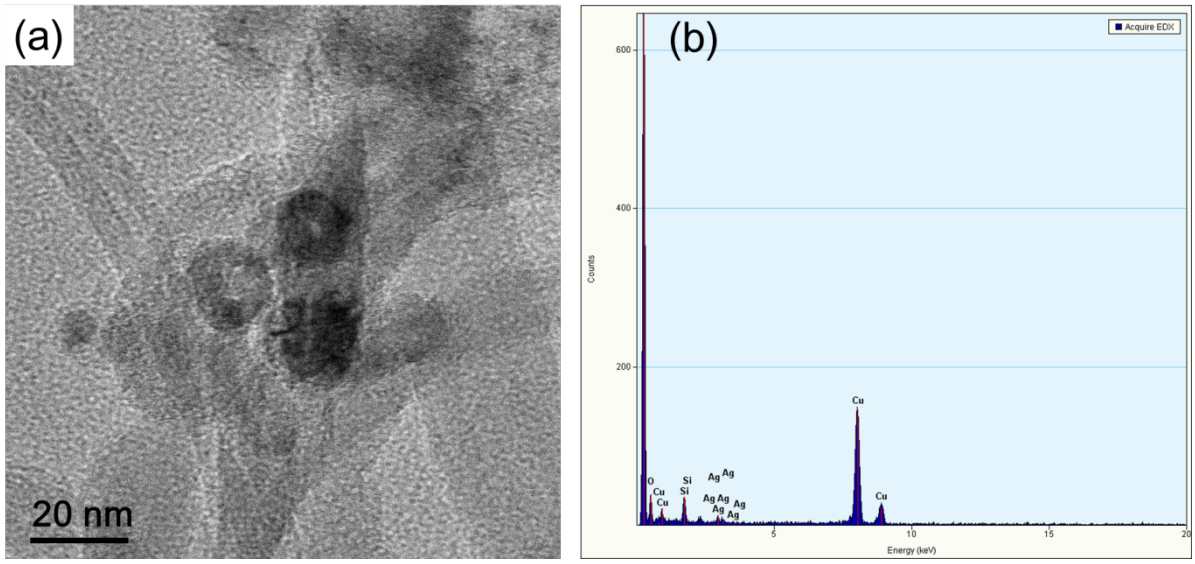

Fig. S9 (a) TEM image of c-CNT after absorption of Ag ion; (b) EDX of c-CNT after binding with Ag^{+} ion.

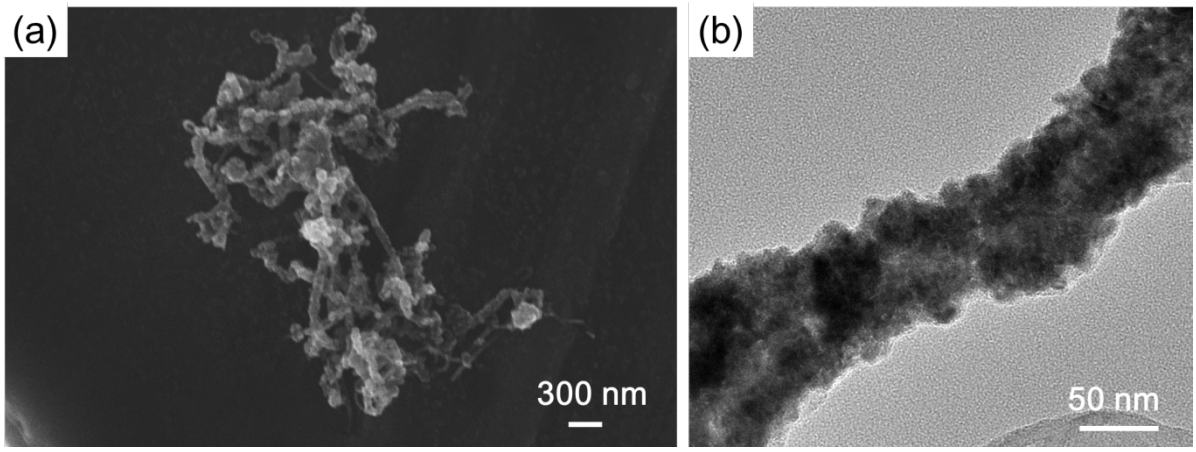

Fig. S10 SEM image (a) and TEM image (b) of CNT@Ni synthesized with the DMAB concentration of 1200 ppm in the ultrasound sonication bath.

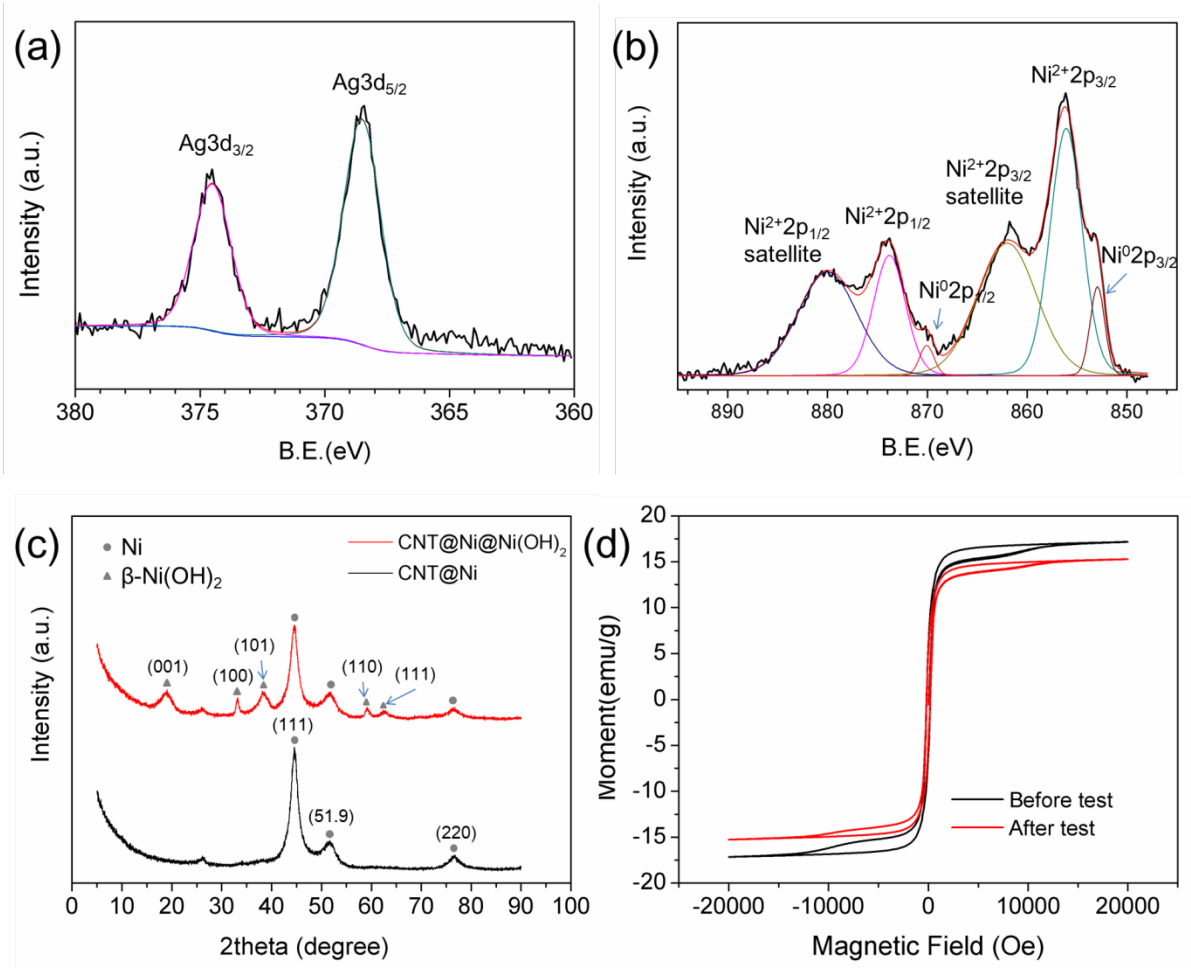

Fig. S11 (a) Ag 3d XPS spectrum of CNT after absorption of silver ions; (b) Ni 2p XPS spectrum of the CNT after electroless deposition of nickel; (c) X-ray diffraction spectroscopy of the CNT@Ni and CNT@Ni@$Ni(OH)_2$; (d) vibrating sample magnetometer (VSM) of the CNT@Ni before and after electrochemical test. The nickel coating on CNT@Ni was characterized by XPS, both the peaks of Ni^0 (853.0 eV and 879.0 eV) and Ni^{2+} (856.1 eV and 873.8 eV) were observed (Fig. S4b), and the presence of the Ni^{2+} peaks could be attributed to the absorbed Ni^{2+} by air auto-oxidized Ni metal. The nickel layer on CNTs was further characterized by X-ray diffraction spectroscopy (XRD), three diffraction peaks with 2θ values corresponding to pristine Ni at 44.6˚, 51.9˚ and 76.4˚ were observed (Fig. S4c). No obvious diffraction peak for Ni^{2+} was found in the XRD spectrum, suggesting that the bulk metal layer of the resulting CNT@Ni was the pristine nickel. After electrochemical test, new peaks with 2θ at 19.3, 33.2, 38.6, 59.1, 62.7˚ appeared, corresponding to the β-$Ni(OH)_2$ layer on CNT@Ni.

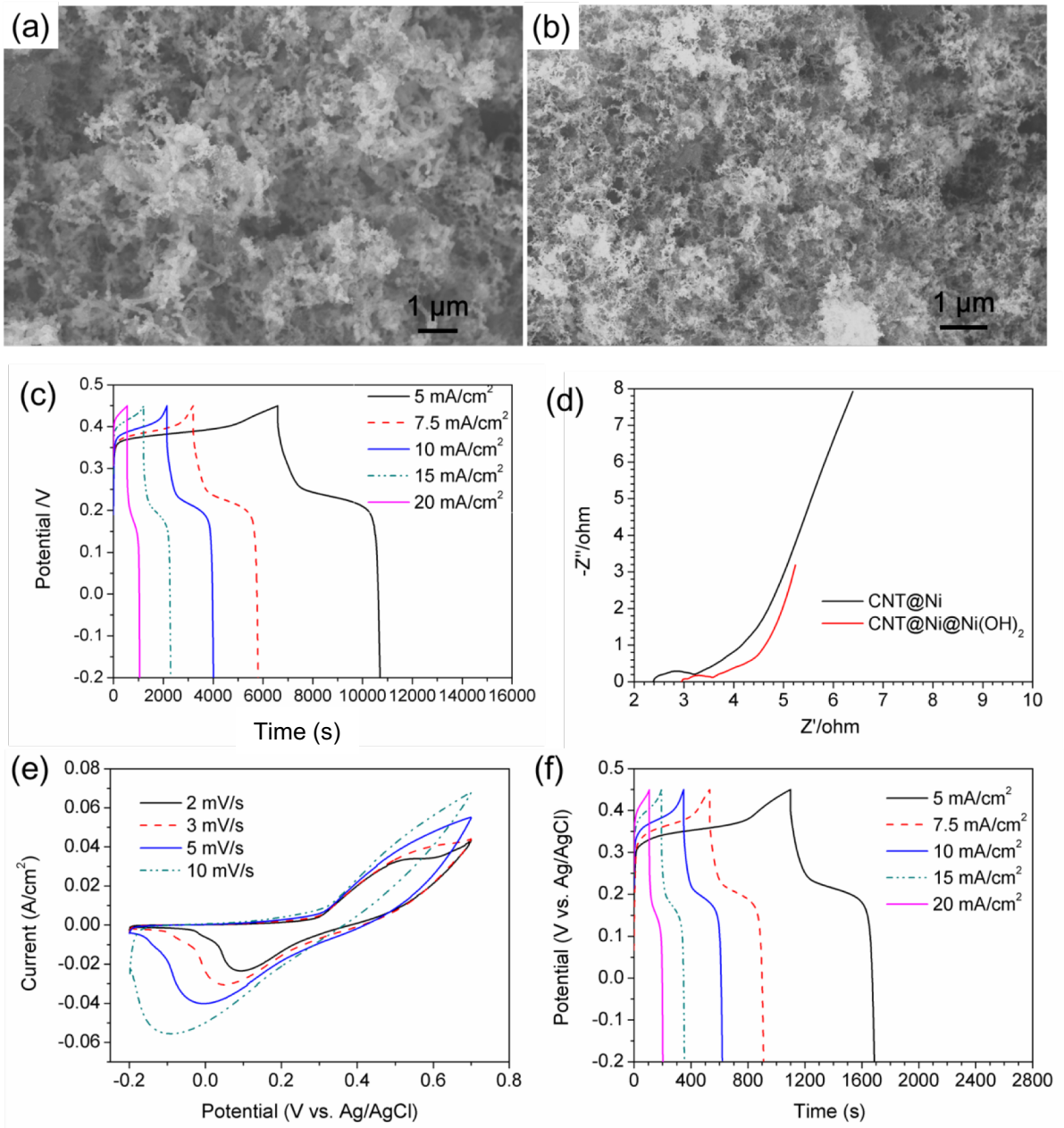

Fig. S12 (a-b) SEM images of the porous CNT@Ni film, (c) GCD curves of porous CNT@Ni film with mass loading 42 mg/cm^2, (d) electrochemical impedance spectra of porous CNT@Ni film before and after GCD test (mass loading 42 mg/cm^2), (e-f) cyclic voltammetry curves and GCD curves of porous CNT@Ni film with a low mass loading of 4.2 mg/cm^2.

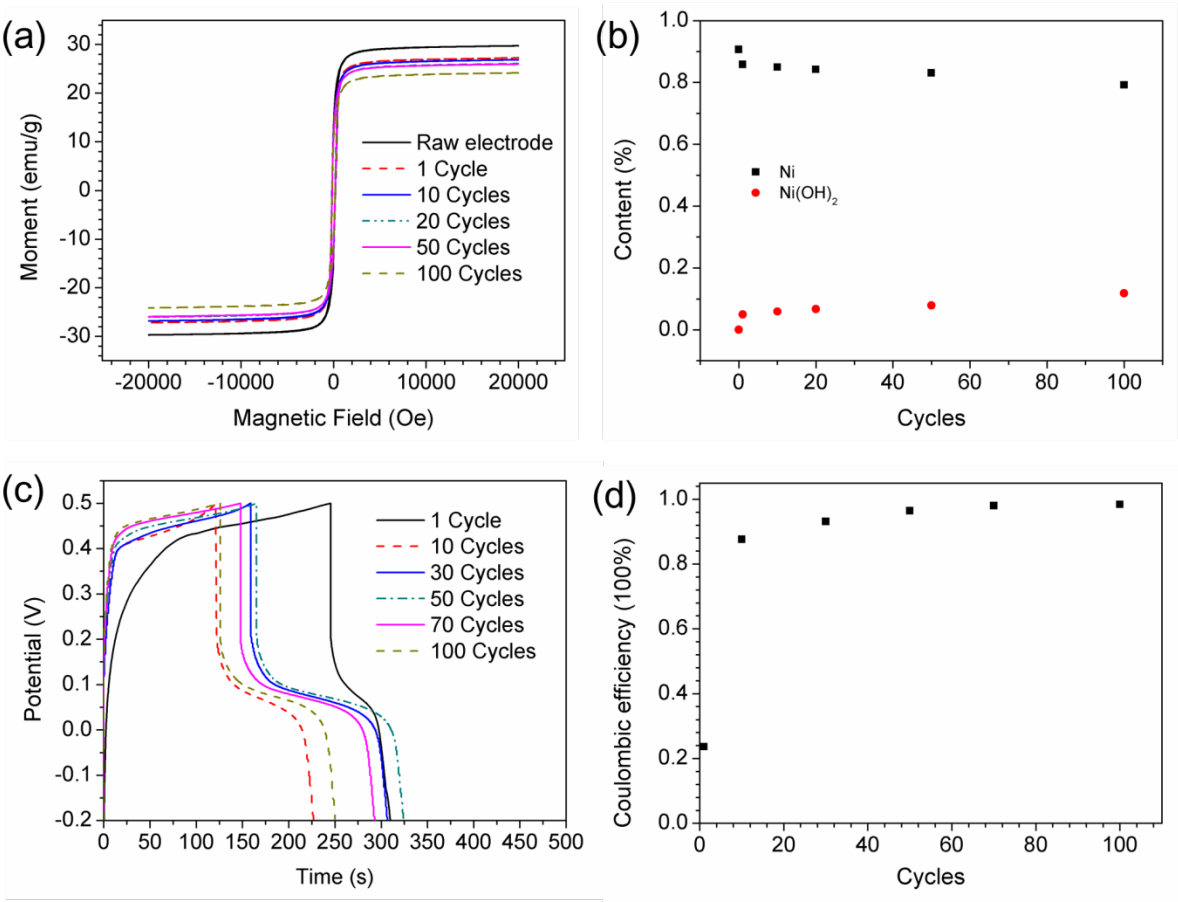

Fig. S13 (a) VSM curves of the porous Ni electrode after GCD test for different cycles, (b) the content of Ni and $Ni(OH)_2$ in the electrode, (c) GCD curves of the electrode at different cycles, (d) coulombic efficiency of the electrode at different cycles.

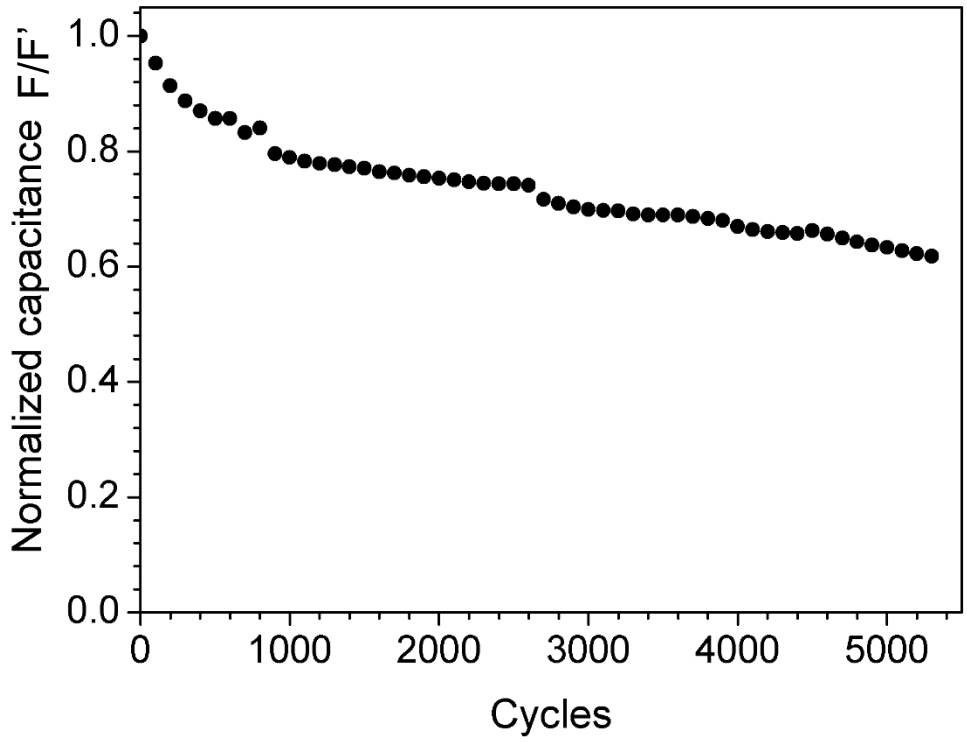

Fig. S14 Long cycle test for freestanding CNT@Ni electrode without curing at high temperature by CV test at a scan rate of 50 mV/s.

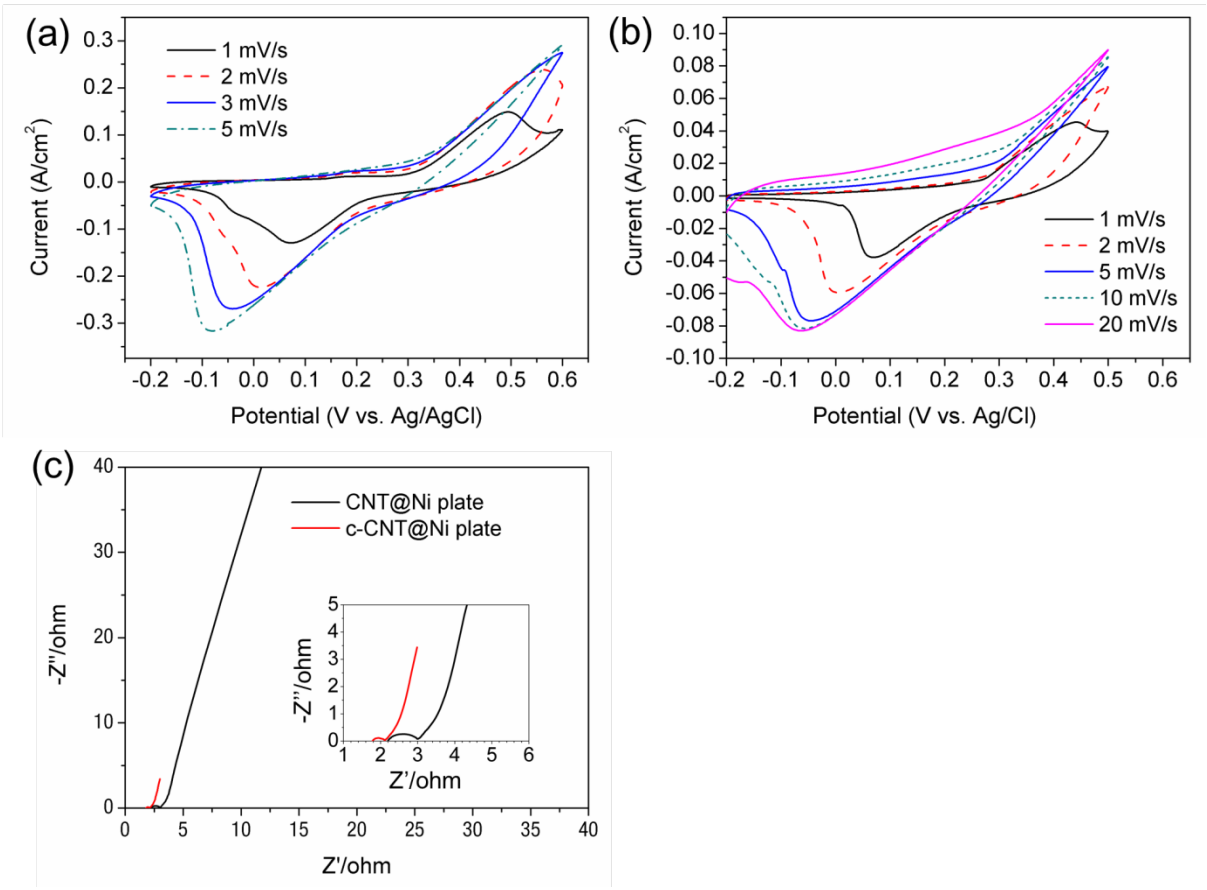

Fig. S15 (a) CV curves of CNT@Ni plate; (b) CV curves of c-CNT@Ni plate; (c) EIS curves of CNT@Ni and c-CNT@Ni electrodes.

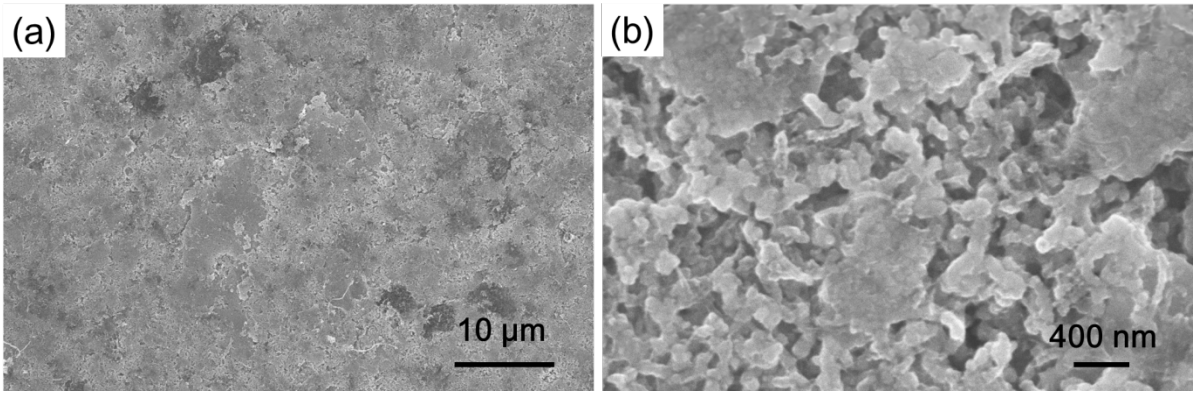

Fig. S16 SEM images of the freestanding CNT-GO@Ni electrode with different scales of magnification.

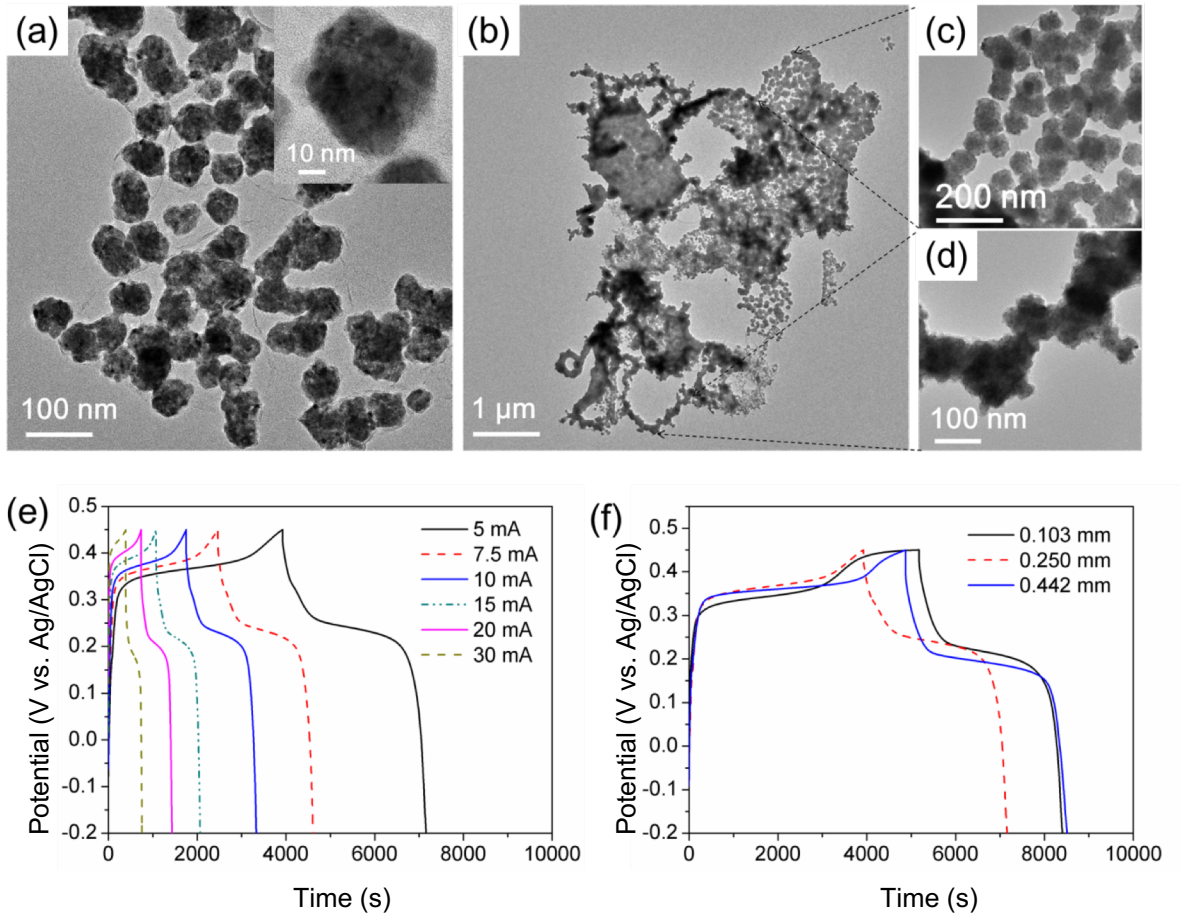

Fig. S17 (a) TEM images of GO@Ni (diameter ~50 nm), (b-d) TEM images of GO-CNT@Ni with different magnifications, (e) GCD curves of GO-CNT@Ni, (f) GCD curves of GO-CNT@Ni plates with different thicknesses at the same current density of 66.5 mA/g(electrode). A freestanding electrode was fabricated using CNT-GO@Ni hybrid materials with the nickel loading of 88%. The electrode had a thickness of 0.250 mm and a density of 3.0 g/cm^3. The electrode had nanoporous structures (Fig. S9), and nickel-coated CNTs in the electrode also had side branches (Fig. 2d). The GCD characterization of CNT-GO@Ni was shown as Figure 5e. The areal capacitances were 26.2, 26.7, 27.0, 27.0, 26.8, 24.7 F/cm^2 at 5, 7.5, 10, 15, 20, 30 mA/cm^2, respectively. Regarding to the density and thickness of the electrode, the specific capacitance and volumetric capacitance of the electrode at the current of 20 mA/cm^2 were 357 F/g and 1074 F/cm^3, respectively. The electrochemical performance of CNT-GO@Ni is comparable to that of CNT@Ni. To explore the scalability of the electrode, the specific capacitance of the electrode with different thickness was characterized by GCD test (Fig. 5f). The electrodes with thicknesses of 0.103, 0.25, 0.442 mm showed increased areal capacitances of 13.02, 26.15, 63.65 F/cm^2, respectively. The three electrodes have comparable volumetric capacitance with the highest value of 1440 F/cm^3.

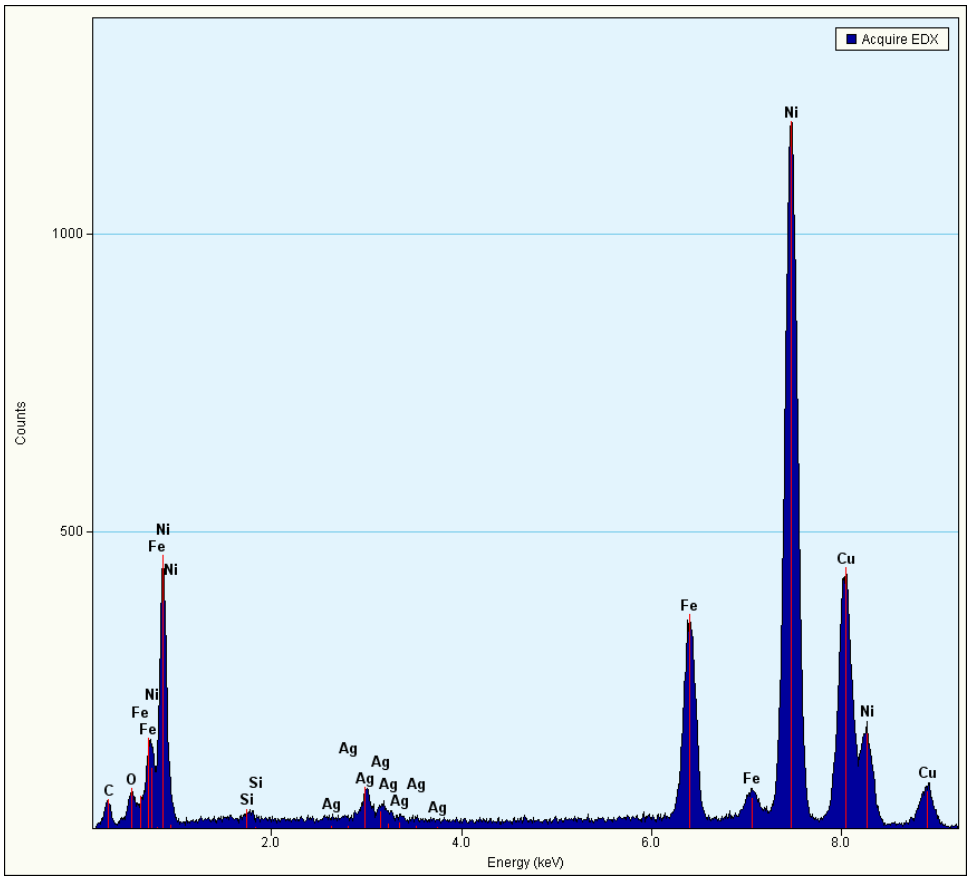

Fig. S18 Energy dispersive X-ray spectroscopy of CNT@Ni-Fe.

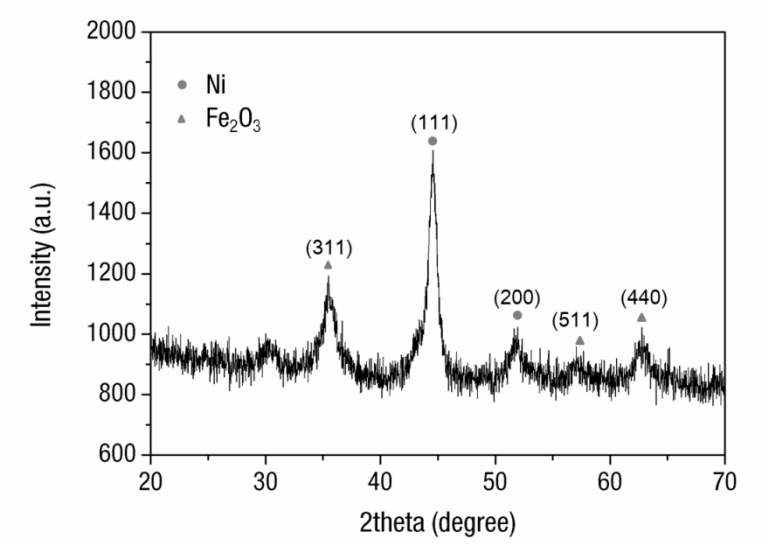

Fig. S19 XRD spectroscopy of CNT@Ni-Fe@Fe_2O_3.

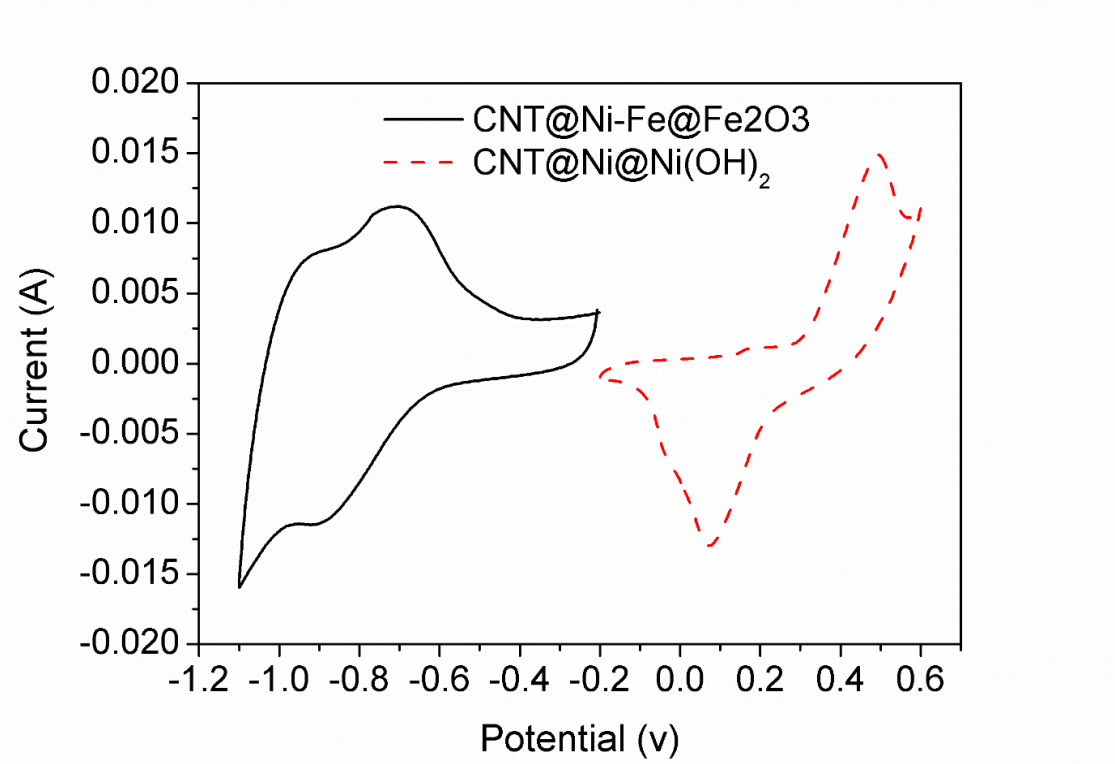

Fig. S20 CV curves of CNT@Ni-Fe@Fe_2O_3 and CNT@Ni@$Ni(OH)_2$ at the scan rate of 1 mV/s.

Section 4: References

1. H. R. Wessels and H. W. Gibson, *Tetrahedron* 2016, **72**, 396-399.

2. M. V. Martínez-Díaz, N. S. Fender, M. S. Rodríguez-Morgade, M. Gómez-López, F. Diederich, L. Echegoyen, J. F. Stoddart and T. Torres, *J. Mater. Chem.* 2002, **12**, 2095-2099.

3. K. Zhu, M. Zhang, F. Wang, N. Li, S. Li and F. Huang, *New J. Chem.* 2008, **32**, 1827-1830.